Global Journal of Engineering and Technology Advances
eISSN: 2582-5003
Cross Ref DOI: 10.30574/gjeta
Journal homepage: https://gjeta.com/

(REVIEW ARTICLE)

Check for updates

Numerical study on the torsional behavior of CFRP-strengthened RC beams

Noha Yehia Elwakkad *

Department of Civil Engineering, Faculty of Engineering, Damahour University, Egypt.

Global Journal of Engineering and Technology Advances, 2023, 17(02), 012–030

Publication history: Received on 26 September 2023; revised on 07 November 2023; accepted on 10 November 2023

Article DOI: https://doi.org/10.30574/gjeta.2023.17.2.0228

Abstract

The present paper offers a numerical study on the behavior of reinforced concrete (RC) beams strengthened with carbon fiber reinforced polymer (CFRP) under pure torsional loading. The failure mode of RC beams significantly changed in accordance with torsional loading. Therefore, the effect of strengthening RC beams by CFRP under torsion is a vital area of study. This paper attempted to fill the gap by conducting a numerical (Abaqus) study, whereby the numerical investigation was in line with the parametric for a previous study of an experimental program. The numerical model achieved agreement with the results of the experimental program, then, this model was used by applying CFRP, instead of GFRP. Additionally, the numerical study was completely in line with the parametric study in terms of sample dimensions, steel reinforcement, number of FRP layers, and width of FRP strips, for the aim of comparing results. The comparative evaluation in this study aims to contrast the behavior of RC beams strengthened by CFRP with the behavior of those strengthened by GFRP under pure torsion. Parameters such as ultimate torsional moment, and the maximum angle of twist were studied. The study revealed that strengthening with CFRP improved the ultimate strength and post-cracking stiffness, in addition to localizing the damage.

Keywords: Torsion Strengthening; Carbon fiber reinforced polymer (CFRP); Torsional capacity; Twist angle; Self-compacting concrete (SCC)

1. Introduction

Fiber reinforced polymers (FRP) is a frequently utilized strengthening materials for RC elements. This is attributed to its numerous vantage points, particularly its light weight, high strength and stiffness, and its ease of application. Unexpected loads, faulty designs, construction errors, changes to type of usage are some of the reasons why existing structures must be strengthened. In contrast with un-strengthened RC members, the behavior of RC members strengthened with FRP (glass and carbon) is rather more intricate. Hence, a thorough examination of such behavior under several loading conditions is essential.

Numerous studies were previously undertaken to better explain the behavior of RC beams strengthened using FRP under flexure and shear [2–7] [2-15]. On the other hand, torsional behavior received little consideration in spite of its common presence in multiple key engineering structures. For both experimental and analytical research, torsion is more p2roblematic than other types of loads [16-18] (Ameli and Ronagh 2007; Salom et al. 2004; Ghobarah et al.). In the majority of cases, torsion is a secondary effect, yet gains utmost significance in connecting beams, outrigger bent, and bridge columns. As a result, it becomes critical to fully comprehend the behavior of RC members under the effect of torsion.

Furthermore, the effectiveness of FRP strengthening when it comes to improving stiffness and strength under torsional loading remains inadequately recognized, because of the complicated impact of FRP on concrete softening, confinement,

* Corresponding author: Noha Yehia Elwakkad

and tension stiffening behavior. By conducting analytical and FE invest-igations, this study aims to fill a gap in the knowledge on such a vital area of study.

The behavior of FRP-enhanced RC beams could be understood when the assembly of membrane elements features extra equilibrium and compatibility conditions. Figure (1) shows the shear flow in the FRP-strengthened RC beam under an external force 'T', and Membrane element 'E' subjected to shear flow 'q.'

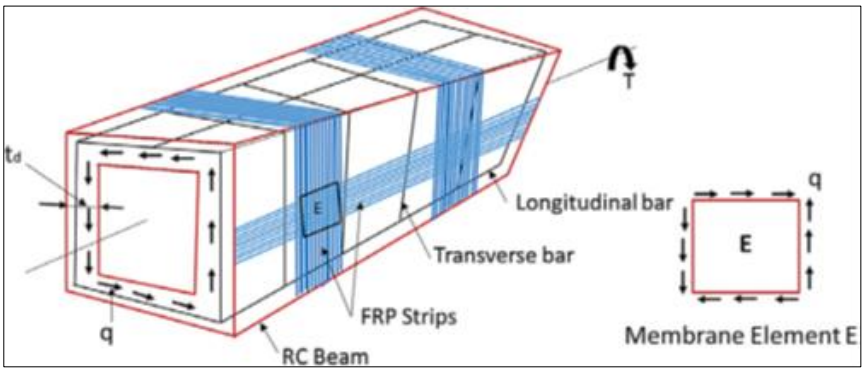

Figure 1 FRP-Wrapped RC Beam under Torsion and Membrane Element E

Few researchers previously studied the behavior of RC members strengthened using FRP under torsional strain. Ghobarah [19] investigated the influence of GFRP and CFRP strengthening on the torsional behavior of RC beams in an experimental study. The wrapping configurations were different. The study reported that the 45-degree fiber orientation offered a higher degree of efficiency in enhancing torsional strength when compared to the 0-degree and 90-degree fiber orientations. In the experimental study by Panchacharam and Belarbi [20], the torsional behavior of RC beams strengthened with FRP was investigated, with the study parameters being fiber orientation, number of layers, and number of strengthened beam faces. The study reported that strengthening using glass fiber reinforced polymer (GFRP) sheets increased the maximum twist angle and ultimate torsional moment. The study also highlighted that the most efficient confinement was achieved with a 90-degree fiber orientation from the beam axis. The experimental study by Ameli et al. [16] investigated the impact of GFRP and CFRP on the torsional behavior of reinforced concrete beams. A numerical study was also conducted using finite element (FE) software (ANSYS), reporting that the FE model represented the ultimate torque with a divergence of less than 13% from the experimental measurements, yet post-crack behavior was not well captured. Mahmoud [21] studied the behavior of 9 half scale RC continuous flat slabs include openings and without openings, noting that the size limit of the openings were in accordance with the Egyptian Code (ECP 203-2007), and ACI 318-19. The RC slabs were strengthened with CFRP. A Finite Element Method (FEM) was applied using the program ANSYS12, the results of which were compared to the experimental results, showing that when RC flat slabs with openings were strengthened using CFRP, slab ductility increased by 28% in contrast with the value recorded by the slab without openings. The numerical results of ANSYS showed that this program can simulate the behavior of CFRP-reinforced RC slabs with openings. Mazloom et al. [22] utilized ABAQUS finite element analysis package to model self-compacting RC girders strengthened with CFRP and GFRP sheets. The numerical results revealed a decline in the stiffness of RC girders with the growth of cracks, and an increased tolerance to extra stresses owing to the adhesive layer, GFRP, and CFRP sheets. Girders with 2 sheets of CFRP exhibited the highest increase in torsion, shear, and bending strengths by 76%, 90%, and 60%, respectively, in contrast with the control beam. The theoretical model offered by Silva et al. [23] for torsion-resistant RC beams strengthened with carbon fiber composites was based on the diagonal compression field theory, and was applied to a mathematical software to identify torsional capacity and angle of twist. Test results obtained from the literature were used to validate the accuracy of the proposed model, which in turn displayed validity. The model also proved to be conservative in determining the torsional capacity of the studied specimens.

The present study provides a numerical investigation of the behavior of eleven self-compact CFRP-strengthened RC beams under torsional load. The study examines the effect of strengthening using CFRP on RC beams subjected to pure torsion with variable strips width, and different number of plies. For this purpose, the implementation of the numerical program is in alignment with the experimental parametric study [1]. When the numerical model achieved agreement with the results of the experimental program [1], the model was applied, but using CFRP instead of GFRP. Additionally, the numerical study adopted the same sample dimensions, steel reinforcement, number of FRP layers, and width of FRP strips of the parametric study, for the aim of comparing results. The comparative evaluation in the present study aims to contrast the behavior of RC beams strengthened by CFRP with the behavior of those strengthened by GFRP under

pure torsion. This investigation uses ABAQUS 6.14 [24]. Hence, the FE analysis is considered an economic investigation since it has the ideal specimens prior to actually carrying out the laboratory experiments, which is the reason behind multiple studies opting to conduct a numerical analysis of structures.

2. Beam Design and Strengthening Specifications

Every beam was created with a steel reinforcement ratio (ρ) of 2.3% to deter failure under flexural and torsional cracking loads. The same reinforcement was used for all the beams, with high tensile steel bars with diameter of 2Φ16 at the bottom, and 2Φ12 mm on top. Mild steel stirrups with diameter of 5 Φ 6 mm were also utilized. The cross-section dimensions and steel reinforcement configurations for each beam are illustrated in Figure (2).

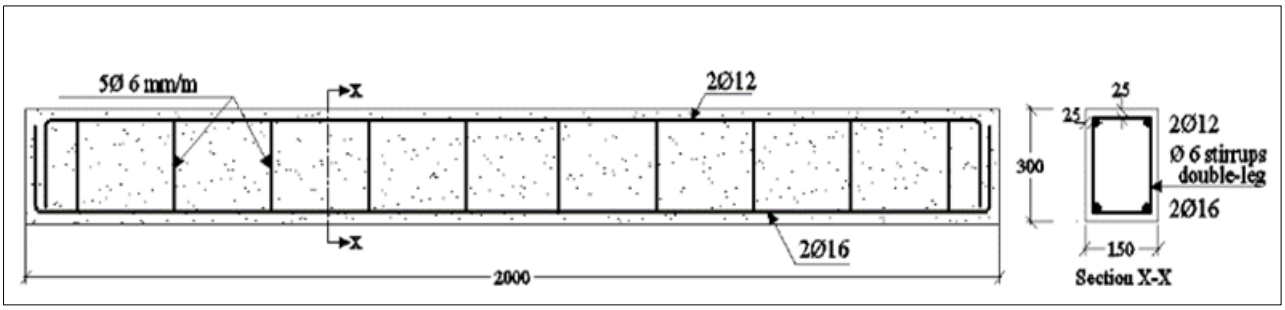

Figure 2 Beam Dimensions and Reinforcement Configurations (in mm)

In addition to one un-strengthened beam (BC-0-0) as the control, 10 beams were strengthened with CFRP wrapping in different configurations. The primary parameters investigated in this experimental study were the number of layers and spacing of CFRP sheets. In 8 specimens, intermittent CFRP strips with width of 50, 125, 150, and 200 mm were employed for strengthening, while the wrapping was applied to surround the beam specimens at a spacing of 100, 250, 300, and 400 mm using 2, 3, and 4 layers. In the remaining 2 specimens, a continuous CFRP wrap was utilized for strengthening, using 2 and 3 layers. All beam specimens were subjected to pure torsion then tested. The details of the tested beam specimens are listed in Table (1). The wrapping arrangement is depicted in Figure (3).

Table 1 Details of Strengthening by CFRP Layers [1]

Group	Beam code	Strengthening layout	Strengthening form	No. of Layers n_f (mm)	Width of CFRP Strips w_f (mm)	Spacing Between CFRP Strips s_f (mm)
Group I (Control)	BC-0-0	—	—	—	—	—
Group II	BC2-150-300	Fully Wrapped	Intermittent strips	2 Plies	150	300
	BC2-200-400	Fully Wrapped	Intermittent strips		200	400
	BC2-1600-0	Fully Wrapped	Continuous strips		1600	0
Group III	BC3-50-100	Fully Wrapped	Intermittent strips		50	100
	BC3-125-250	Fully Wrapped	Intermittent strips		125	250
	BC3-150-300	Fully Wrapped	Intermittent strips		150	300
	BC3-200-400	Fully Wrapped	Intermittent strips		200	400

	BC3-1600-0	Fully Wrapped	Continuous strips		1600	0
Group IV	BC4-150-300	Fully Wrapped	Intermittent strips	4 Plies	150	300
	BC4-200-400	Fully Wrapped	Intermittent strips		200	400

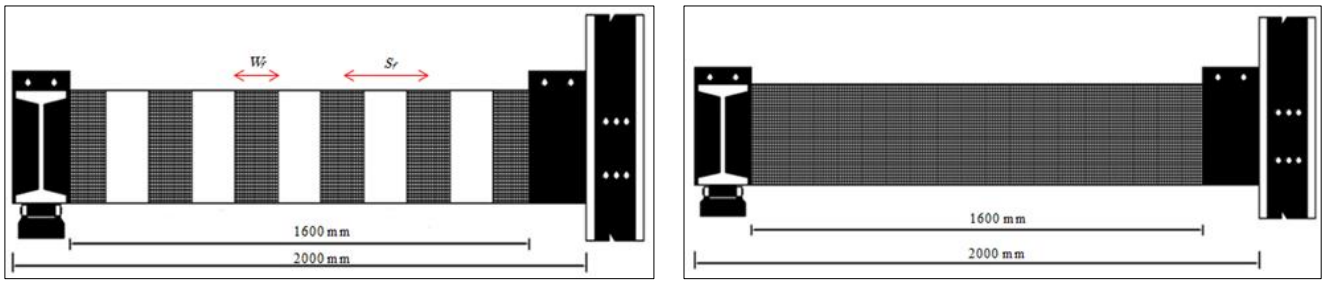

(a) Intermittent CFRP Strips (b) Continuous CFRP Strips

Figure 3 CFRP Strips Arrangement [1]

3. Finite Element Modeling

FE modelling of self-compact RC beams strengthened with FRP, such as CFRP, is challenging because it reacts to several nonlinear behaviors, including steel yielding, concrete plasticity, cracking, crushing, FRP rupture, and FRP debonding. Important FE investigations were previously conducted on RC beams subjected to shear and flexure [25-27]. However, a limited number of studies focused on the behavior of RC beams under torsion using FE analysis [16, 28, 29]. In this study, a nonlinear FE model was developed to predict torsional behavior of RC beams strengthened by CFRP using ABAQUS for different parameters.

3.1. Element Description

For the construction of the FE model, a three dimensional FE mesh of concrete beams, reinforcement bars, and CFRP strengthening sheets were created by means of three main types of elements, namely, solid, truss (wire element), and shell elements.

3.1.1. Solid Element

C3D8R or the brick element displayed in Figure (4) was used to model concrete beams as recommended by Ibrahim Alshaikh et al. [30–32], and Zhao and Li [33]. The element's nodes had three transitional degrees of freedom. This element was selected because it could specify the concrete beam property's bounds, as well as the contact faces required to apply load and CFRP strengthening, and to define boundary conditions. Furthermore, it corresponded with accuracy to the constitutive law integration, and was ideally suitable for nonlinear static and dynamic analysis, as well as for large displacement analysis with finite rotation and strain. Besides, roller supports, and line-x coating were designated with C3D8R element. Figures (5 & 6) demonstrate the created pieces.

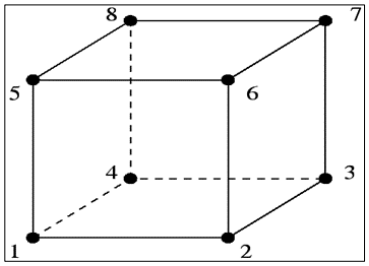

Figure 4 8 Node three Dimensional Solid (Brick) Element

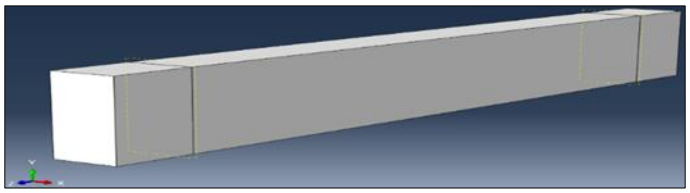

Figure 5 Concrete Beam Part

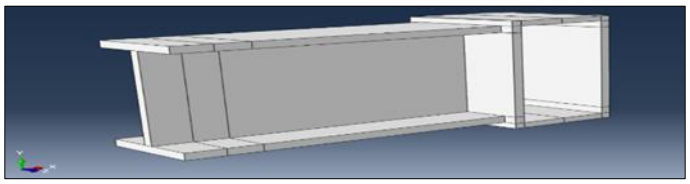

Figure 6 Steel Arm Part

3.1.2. Truss Element

Figure (7) illustrates the selection of T3D2 element to model reinforcement bars and stirrups, modeled as embedded elements in the concrete block.

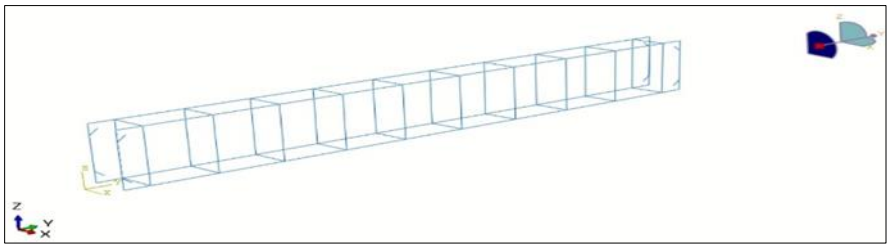

Figure 7 Steel Reinforcement Bars and Stirrups Modeled with Truss Element

3.1.3. Shell Element

The collection of shell element in Abaqus included elements that could be of use to represent curved, intersecting shells with nonlinear material responses, and significant overall motions, i.e., translations and rotations. Additionally, these shell elements could simulate composite bending behavior. To model CFRP, the conventional shell type was used. There were also elements to model structures, in which one of the dimensions or thicknesses was significantly lower than others. Such condition was employed by conventional shell elements for the purpose of discretizing a body, by means of defining the geometry at a reference surface. Section property definition was, thus, used to define thickness. In 3D space, conventional shell elements required a two-dimensional geometry. Thick and thin shell elements (S8R and S8R5) were samples of the traditional shell elements. Whereas thin shell elements had five degrees of freedom (DOF) per node, thick shell elements had six DOF per node. Figure (8) displays the CFRP parts that were created using the conventional shell element type.

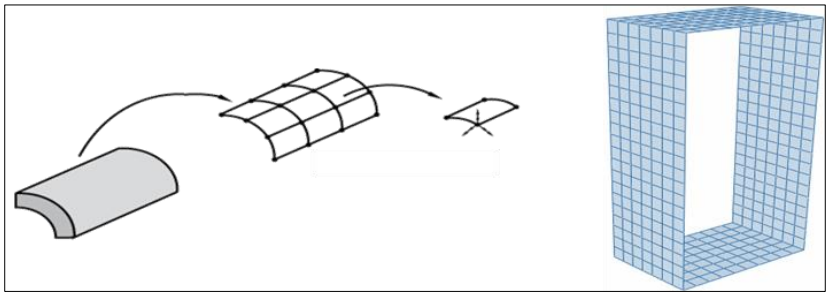

Figure 8 Modeling of CFRP with Conventional Shell Elements

In the current models, element of size 12 ×12 ×12 mm was chosen for the concrete beam and CFRP sheets, except for a steel arm of size 20 x 20 x 20 mm, as shown in Figure (9)

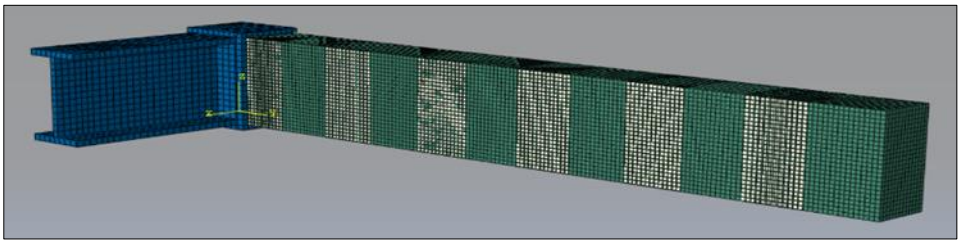

Figure 9 Mesh Configuration of FEM model

3.2. Material Modeling

The material properties of all elements were defined. Nevertheless, it was challenging to obtain high-quality material data, specifically in the case of complicated material models, such as material damage properties. Validity of the results relied mostly on the correctness and scope of the material data. To model the RC beams, three material models were employed, namely: the damaged plasticity model for concrete, utilized to model the concrete; the elastic-plastic model, utilized to model the steel reinforcement bars embedded in the concrete elements; and the elastic-lamina model, utilized to model CFRP sheets.

3.2.1. Concrete Damaged Plasticity Model (CDP)

The material model for concrete was a plasticity-based, continuum, damaged model. As demonstrated in Figure (10), damaged plasticity was the main characterizing factor of the concrete's uniaxial compressive and tensile response. The stress-strain curve showed linear elasticity under uniaxial tension since the beginning, and until reaching failure stress (Ft0), in line with ABAQUS user guide (2013). Failure stresses were transformed into micro cracks within the concrete blocks. Figure (10.a) demonstrates that the stress-strain response was presented with softening characteristic beyond the condition of failure stress in concrete. The uniaxial compression response was linear to the point of reaching the initial yield value (Fc0). Figure (10.b) illustrates that the response of the concrete was characterized by stress hardening followed by strain softening upon arriving at the ultimate stress (Fcu) within the plastic zone.

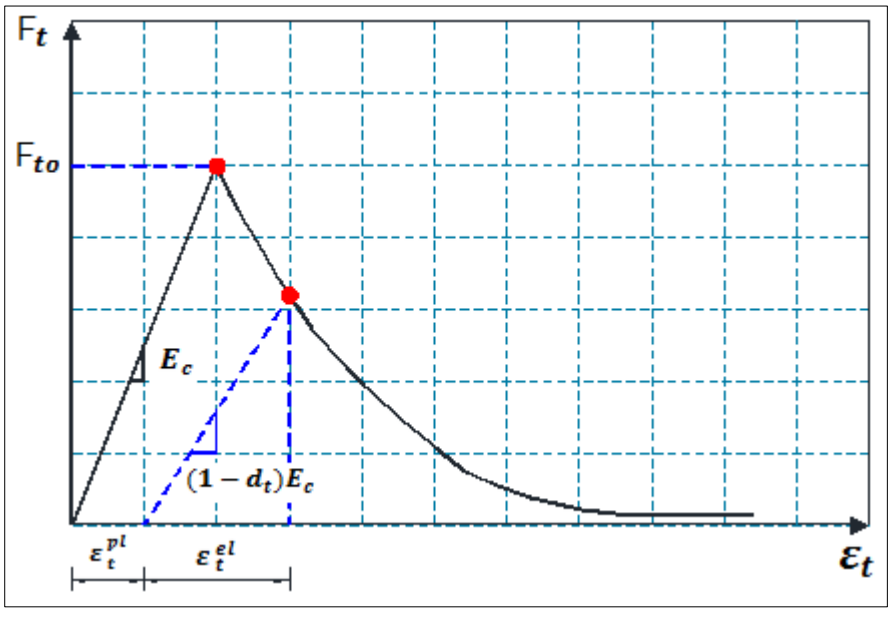

(a)Tension Behavior Associated with Tension Stiffening

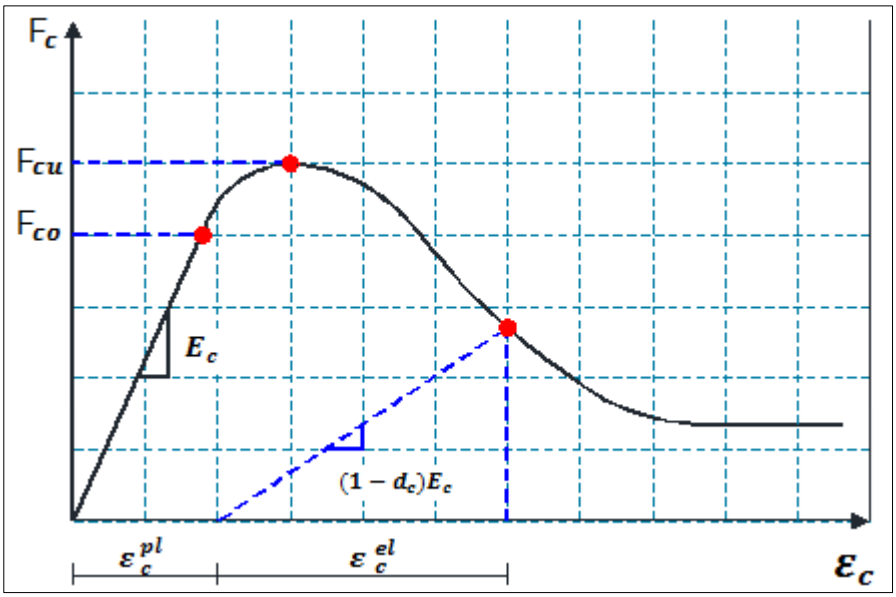

(b) Compressive Behavior Associated with Compression Hardening.

Figure 10 Damaged Plasticity of Concrete [24]

The post-failure behavior of RC was represented by the post-failure stress as a function of cracking strain $\varepsilon_t^{c\,k}$ and $\varepsilon_c^{c\,k}$, defined as the total strain minus the elastic strain corresponding to the undamaged material. Data of tension stiffening were specified with regard to cracking strains, in line with ABAQUS user guide (2013).

Tables (2 & 3) list the concrete's elastic characteristics and the parameters of the concrete damaged plasticity model utilized in the study.

Table 2 Concrete Elastic Properties

Parameter	Value
Density, kg/m^3	2200
Modulus of elasticity (E_c), MPa	25685
Poisson's ratio (v)	0.2

Table 3 Parameters of Concrete Damaged Plasticity

Parameter	Value
Dilation angle	40^o
Eccentricity	0.11
fb0/fc0	1.36
K	0.68
Viscosity parameter	0.00000001
Compressive ultimate stress	35 MPa
Tensile failure stress	3.5 MPa

3.2.2. Elastic-plastic Model

Steel reinforcing bars had an almost linear elastic behavior when steel stiffness was constant at low strain values, following Young's modulus. At greater strain values, the bars began to show nonlinear inelastic behavior, which is referred to as plasticity. The yield point and post-yield hardening of steel characterized the plastic nature. The transition from elastic to plastic behavior took place at the yield point as denoted on the stress-strain curve. When the steel was deformed before reaching the yield point, there were only elastic strains created, and were entirely recovered when the load applied was removed. However, when the steel's stress reached the yield stress point, plastic, i.e., permanent, deformation occurred. When the steel was deformed in the post-yielding zone, both elastic and plastic strains increased. As soon as the material yielded, a decrease in steel stiffness was noticed. In addition, an increase in yield stress during subsequent loadings was observed as a result of the steel's plastic deformation. To represent primary longitudinal reinforcement beam bars, high tensile bars with diameter of 10 mm were employed, whereas to represent beam stirrups, typical mild bars with diameter of 6 mm were employed. Table (4) shows the properties of steel reinforcement used to model longitudinal bars and stirrups.

Table 4 Properties of Steel Reinforcement

Parameter	High Tensile	Normal mild
Density, kg/m3	7860	7860
Modulus of elasticity (Es), MPa	210000	205000
Poisson's ratio (υ)	0.3	0.3
Yield stress, Mpa	367.5	255
Ultimate stress, Mpa	535	375
Elongation %	15.89	24.79

3.2.3. Elastic-lamina Model

Carbon fiber was modeled as orthotropic elastic lamina. This model consisted of multiple layers of conventional shells, as aforementioned. Every ply or layer had a different thickness. Besides, the reinforcement fibers of every layer were differently oriented. The material constants of the fibers were accurately determined, and the lamina material defined under plane stress conditions. Table (5) shows that Abaqus applied the characteristics by means of Poisson ratio (Nu12), Young modulus (E1, E2), shear modulus (G12, G13, G23), and stress limit (sub option-fail stress) in individual axes and planes. For material definition, the values of constants were inserted into the software, either typed in using the data sheets or calculated using software.

Table 5 Properties of CFRP Sikawrap-230 C [34]

Parameter	Value
Density, kg/m3	1820
Modulus of elasticity (E1), MPa	230000
Modulus of elasticity (E2), MPa	230000
Poisson's ratio (Nu12)	0.23
Shear modulus (G12), Mpa	7800
Shear modulus (G13), Mpa	7800
Shear modulus (G23), Mpa	7800
Stress limit (tensile strength), Mpa	4000
Thickness (mm)	0.129

Constructing a new coordinates system was not essentially needed because the coordinates system, as per which the fibers were to be orientated, was similar to the global coordinates system. The coordinates system was defined because the materials were direction-oriented, and the coordinates system orientation was provided to the model.

Consequently, ABAQUS appropriately aligned the material properties. Long-fibered composites with orthotropic characteristics featured three mutually-perpendicular planes with symmetrical material properties. The planes were defined by material axes that were pairs of orthogonal axes labelled 1, 2, and 3. As illustrated in Figure (11), axis 1 was parallel to the direction of the fibers, whereas axes 2 and 3 were perpendicular to the fibers. The direction of axis 1 exhibited the greatest strength (Ref 1).

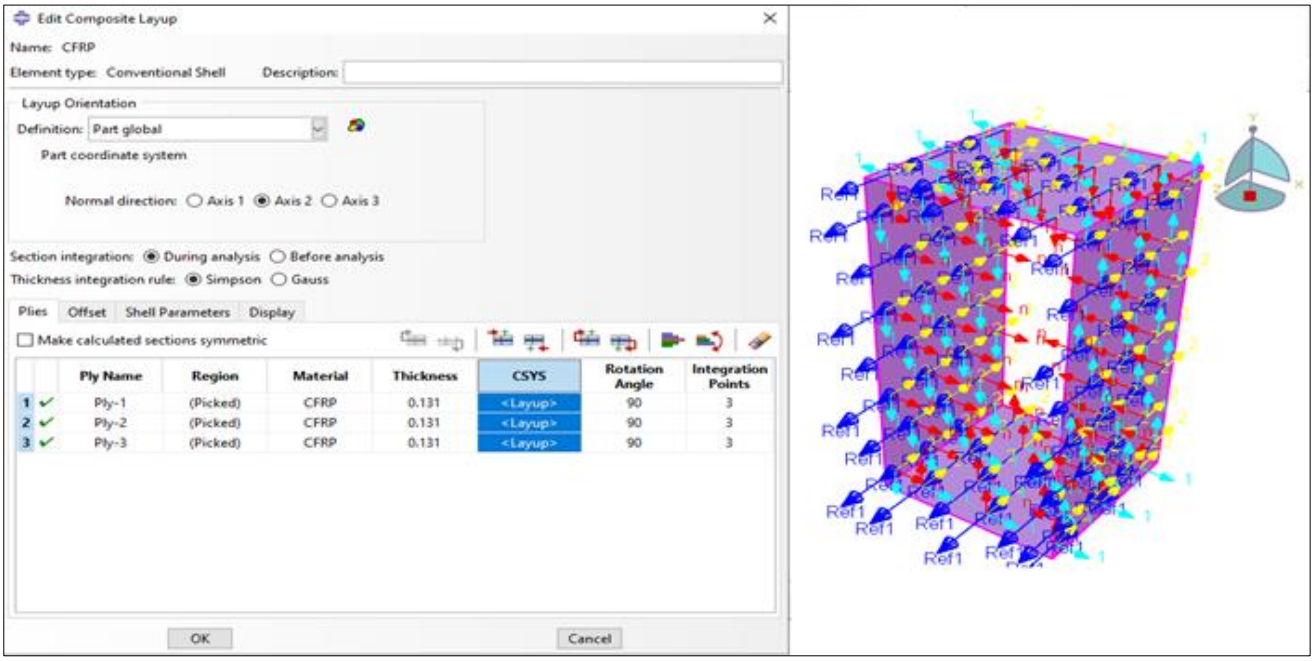

Figure 11 Definition of Coordinates System of CFRP Shell

Assigning materials to the geometry of the model necessitated specifying the number and thickness of layers in the lamina, the material employed, and the orientation of the model to the coordinate system. As per the selected coordinates system, individual layers were assigned to the reference area (chosen). The material, thickness, and orientation of the individual layers were marked, in addition to their positions (over or under) in relation to the reference area.

3.3. Step Definition

Abaqus CAE supports many methods of analysis, such as static, dynamic, thermal, impact, and explosions analyses. The standard/static analysis step was chosen with the suitable periodic time and nonlinear geometry analysis as to represent the most suited case for the behavior of the tested samples. Such module also determined the output control of the analysis results, where the reaction forces, displacement, compression damage, and tension damage of concrete were selected.

3.4. Boundary Conditions

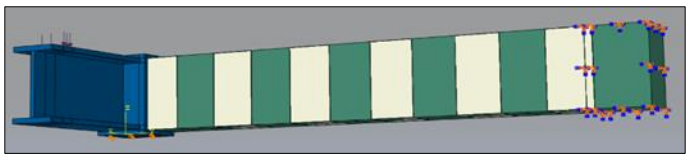

Figure 12 Model's Simply-Supported Boundary Condition

To create and apply boundary conditions to a Model Tree in Abaqus, Loading then Creating boundary condition were selected. Additionally, a fixation with length value of 200 mm in all directions was applied on the right side of the beam section. The fixation demonstrated the fixed support on the ride side of the beam, and was added for the purpose of achieving the closest behavior feasible to the studied samples. A prevention was introduced to deter the left side of beam from translation only in Z direction. As illustrated in Figure (12), the prevention was a line of a length value of

200 mm that was added to the lower side of the steel arm, in order to simulate the roller support condition that hindered vertical movement yet allowed other movements.

3.5. Contact Definition

Contact surfaces could be defined as the interaction between the RC beam and the loading plate using the options "Interaction," "Create Interaction Property," and "Create Interaction." All the parts of the model that could potentially come in touch with each other were defined by creating contact surfaces, as depicted in Figure (13).

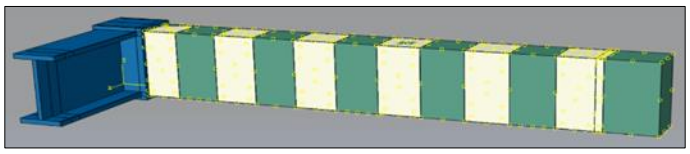

Figure 13 Model Contact Interaction

3.6. Constraint Definition

This form of interaction is known as constraint, and it could be defined by utilizing the options "Interaction," "Create Constraint," and "Embedded Area" to define the interactive relationship between the RC beam and the steel reinforcement. Figure (14) indicates the RC beam as the host region, and all the regions of steel reinforcement as embedded regions.

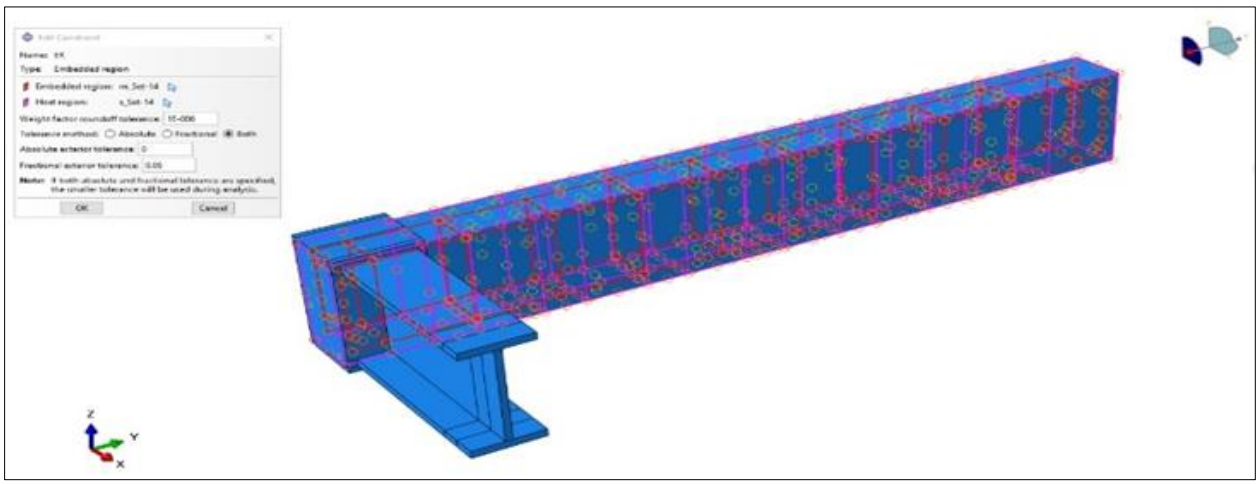

Figure 14 Constraint Definition of Steel Reinforcement

3.7. Creating Job in Abaqus

Option "Create Job" was used to offer direct integration of static stress/displacement response in Abaqus/CAE analysis. To validate, the time of each step was first defined in Abaqus, as explained in the definition section. Figure (15) depicts the Abaqus being used to define a job.

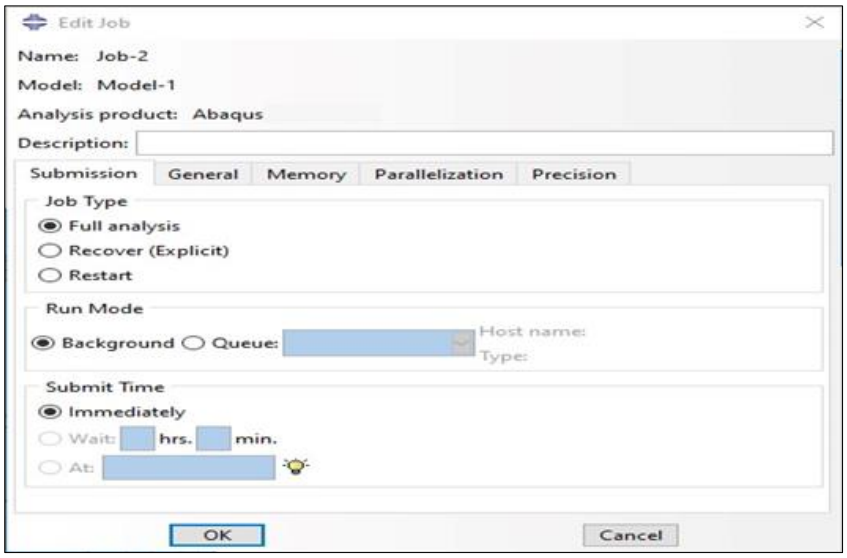

Figure 15 Job definition in Abaqus Environment

4. FEM Simulation Results

4.1. Torsional moment – twist angle

Torsional moment-twist angle relationships (θ) appeared in all the studied specimen. During initial loading, beam BC-0–0 exhibited an almost linear behavior until reaching an angle of twist of 0.00299 rad, marking 15.66% of the maximum twist angle, then adopted a parabolic behavior until failure at an angle of twist of 0.0191497 rad, and ultimate torsional moment of 11.428 kN.m. Beam BC3–125–250 exhibited an almost linear behavior until reaching an angle of twist of 0.003823493 rad, marking about 7.85% of the maximum twist angle, then adopted a parabolic behavior until failure at an angle of twist of 0.04865484 rad, and ultimate torsional moment of 16.66 kN.m. Upon comparison with the values recorded by the control specimen, BC3–125–250 showed an improvement in torsional capacity by 145.83%, and a decrease in the maximum angle of twist by 52.8%, under the same level of loading. Beam BC2–150–300 failed at an angle of twist of 0.053055111 rad, and ultimate torsional moment of 15.11 kN.m, thus showing an improvement in torsional capacity by 132.2%, and a decrease in the maximum angle of twist by 78.3%. As for beam BC3–150–300, failure was reached at an angle of twist of 0.068996889 rad, and ultimate torsional moment of 16.908 kN.m, under the same loading conditions, showing an improvement in torsional capacity by 147.95%, and a decrease in the maximum angle of twist by 84.15%. Beam BC4–150–300 failed at an angle of twist of 0.071178667 rad, and ultimate torsional moment of 17.339 kN.m, thus showing an improvement in torsional capacity by 151.72%, and a decrease in the maximum angle of twist by 66.7% of the maximum twist angle of the control specimen, for the same loading conditions.

In addition, BC2–200–400 failed at an angle of twist of 0.057288 rad, and ultimate torsional moment of 15.51 kN.m, thus showing an improvement in torsional capacity by 135.74%, and a decrease in the maximum angle of twist by 89.9% of the respective values of ultimate torsional moment and twist angle recorded by the control specimen for the same level of loading. Beam BC3–200–400 failed at an angle of twist of 0.0624944 rad, and ultimate torsional moment of 16.48 kN.m, showing an improvement in torsional capacity by 144.28%, and a decrease in the maximum angle of twist by 76.13%. In beam BC4–200–400, failure was reached at an angle of twist of 0.07349 rad, and ultimate torsional moment of 17.3 kN.m, thus showing an improvement in torsional capacity by 151.44%, and a decrease in the maximum angle of twist by 75.1%. BC3–50–100 failed at an angle of twist of 0.066192 rad, and ultimate torsional moment of 17.607 kN.m, thus showing an improvement in torsional capacity by 154.07%, and a decrease in the maximum angle of twist by 60.7%. In beam BC2–1600–0, failure was reached at an angle of twist of 0.054105 rad, and ultimate torsional moment of 17.28 kN.m, showing an improvement in torsional capacity by 151.21%, and a decrease in the maximum angle of twist by 38.9%. BC3–1600–0 failed at an angle of twist of 0.0612039 rad, and ultimate torsional moment of 19.21 kN.m, thus showing an improvement in torsional capacity by 168.14%, and a decrease in the maximum angle of twist by 33.6%.

Furthermore, for the beams strengthened with 2, 3, and 4 plies, the comparison results show that under the same loading conditions the maximum angle of twist decreased from 20% to 42.7%, from 22.95% to 62.72%, and from 25.73% to 27.94%, respectively. Upon comparison with the control beam BC-0–0, results reveal that the ultimate

torsional moment improved by 35.7%, 54.07%, and 51.7%, respectively. In addition, the results of the comparison between beams strengthened with strips of widths of 150 mm and 200 mm under the same loading conditions show that the maximum angle of twist decreased from 21.4% to 58.2%, and from 20% to 53%, respectively. Upon comparison with the control specimen BC-0–0, results reveal an improvement in the ultimate torsional moment by 51.7% and 51.4%, respectively. Comparing the specimens strengthened with spacings (Sf) of 100, 250, 300, and 400 mm between strips, results reveal that the maximum angle of twist decreased 39.27%, 47.17%, from 15.8% to 33.28%, and from 10.08% to 24.89%, respectively, under the same loading level, whereas the ultimate torsional moment improved by 54.07%, 45.83%, 51.7%, and 51.44%, respectively, in comparison to the control beam BC-0–0. Figure (16) shows torsional moment-twist angle relationships of all the specimens under study. The finite element results are demonstrated in Table (6), comparing the ultimate torsional moments and maximum twist angles of all the beams tested.

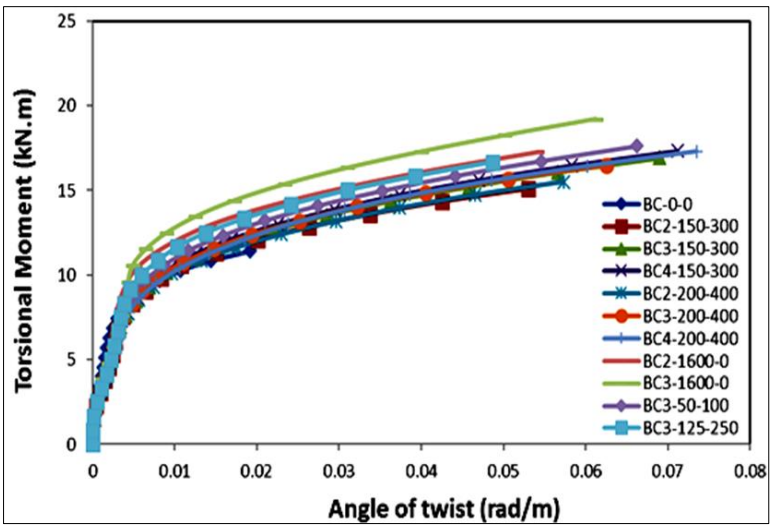

Figure 16 Torsional Moment Versus Twist Angle for the Studied Specimens

Table 6 Finite Element Results

Specimen	**Cracking Load (kN)**	**% Gain in cracking load**	**Ultimate Load (kN)**	**% Gain in Ultimate load**
BC-0-0	14.85	-	22.856	-
BC3-125-250	18.33216	23.45	33.33	45.83
BC2-150-300	13.60024	-8.42	30.222	32.23
BC3-150-300	13.52728	-8.91	33.816	47.95
BC4-150-300	13.87216	-6.58	34.678	51.72
BC2-200-400	13.96144	-5.98	31.02504	35.74
BC3-200-400	14.83984	-0.07	32.97704	44.28
BC4-200-400	15.57648	4.89	34.614	51.44
BC3-50-100	15.84648	6.71	35.214	54.07
BC2-1600-0	20.73664	39.64	34.56	51.21
BC3-1600-0	21.13704	42.34	38.43	68.14
Specimen	**Max Twist A. (rad/m`)**	**% Gain in θu**	**Torsional Moment (kN.m)**	**% Gain in Tult.**
BC-0-0	0.01914978	-	11.428	-

BC3-125-250	0.048654844	154.08	16.665	45.83
BC2-150-300	0.053055111	177.05	15.11	32.22
BC3-150-300	0.068996889	260.30	16.908	47.95
BC4-150-300	0.071178667	271.69	17.339	51.72
BC2-200-400	0.057288978	199.16	15.51252	35.74
BC3-200-400	0.0624944	226.35	16.48852	44.28
BC4-200-400	0.073491467	283.77	17.307	51.44
BC3-50-100	0.066192089	245.65	17.607	54.07
BC2-1600-0	0.054105422	182.54	17.28	51.21
BC3-1600-0	0.061203911	219.61	19.215	68.14

4.2. Cracking and failure pattern

Figures (17-27) represent the failure pattern of all beams, revealing the tension damage of the FE model. These figures clearly show that the primary mode of failure was twisting. Uninterrupted cracks formed a spiral that surrounded the beam's outer circumference. In tension damage contour plots, a value of zero indicated concrete elasticity, a value between zero and 0.5 indicated the formation of microcracks towards the beginning of concrete yield, a value between 0.5 and 1 indicated crack formation, while a value above 1 indicated full concrete failure. It is noteworthy that selecting a fine enough mesh for FE models adequately exhibits the deformation and failure pattern of the samples.

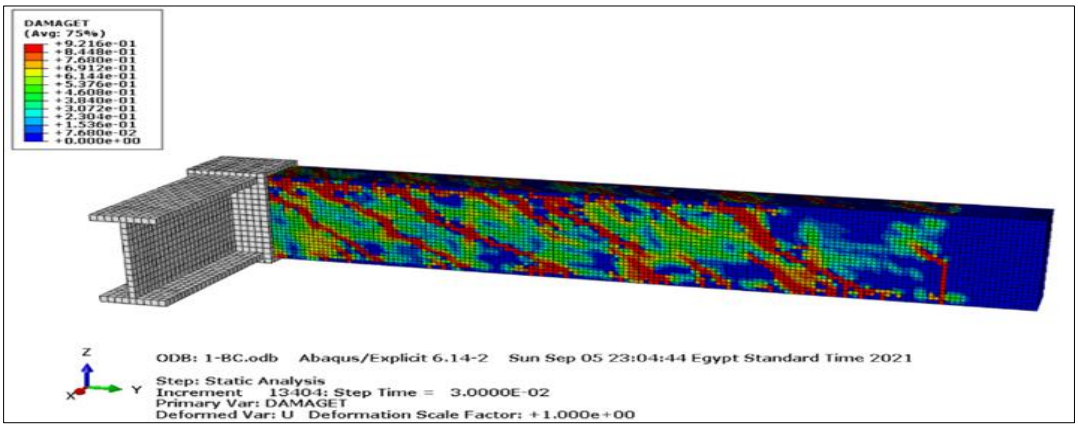

Figure 17 Failure Pattern of FE Model for Control Beam BC

Figure 18 Failure Pattern of FE Model for Strengthened Beam BC3-125-250

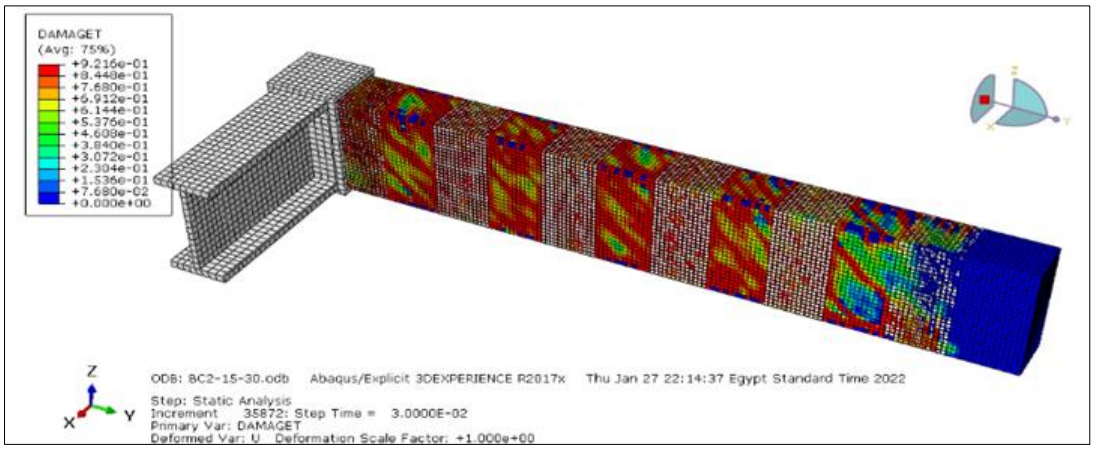

Figure 19 Failure Pattern of FE Model for Strengthened Beam BC2-150-300

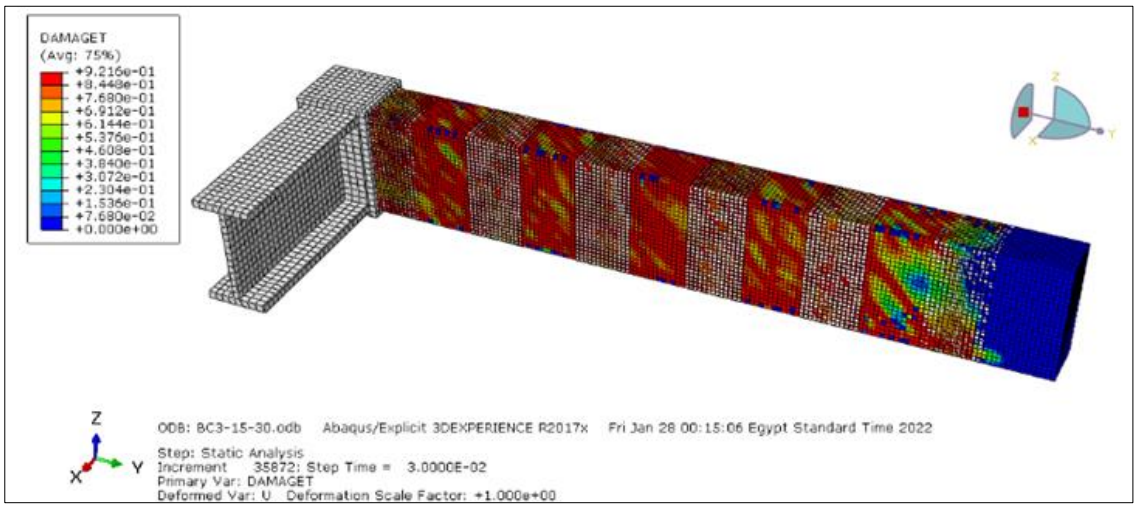

Figure 20 Failure Pattern of FE Model for Strengthened Beam BC3-150-300

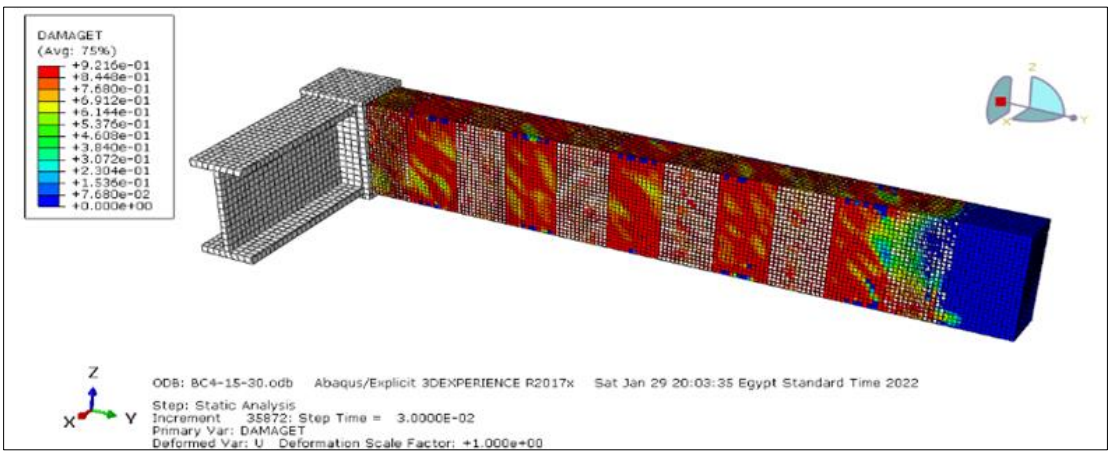

Figure 21 Failure pattern of FE model for strengthened beam BC4-150-300

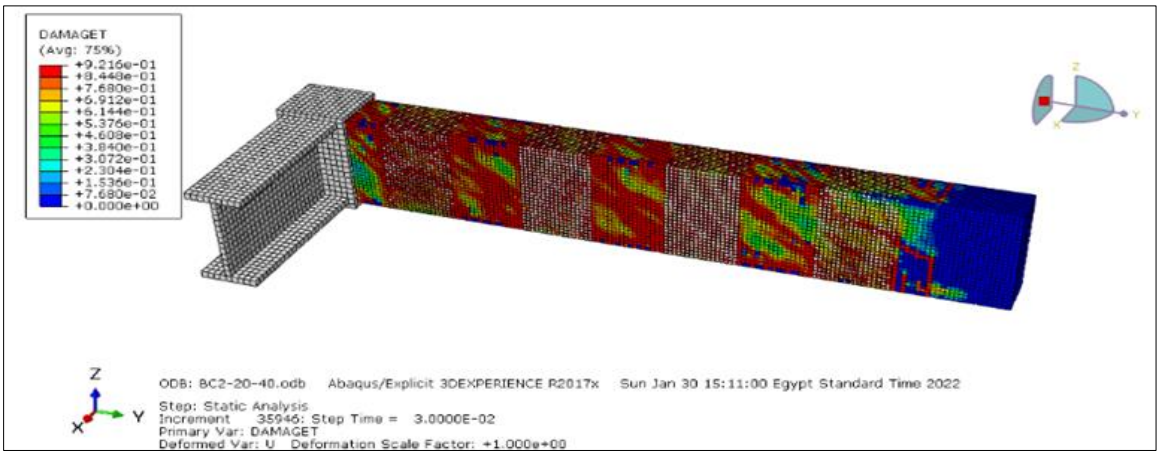

Figure 22 Failure Pattern of FE Model for Strengthened Beam BC2-200-400

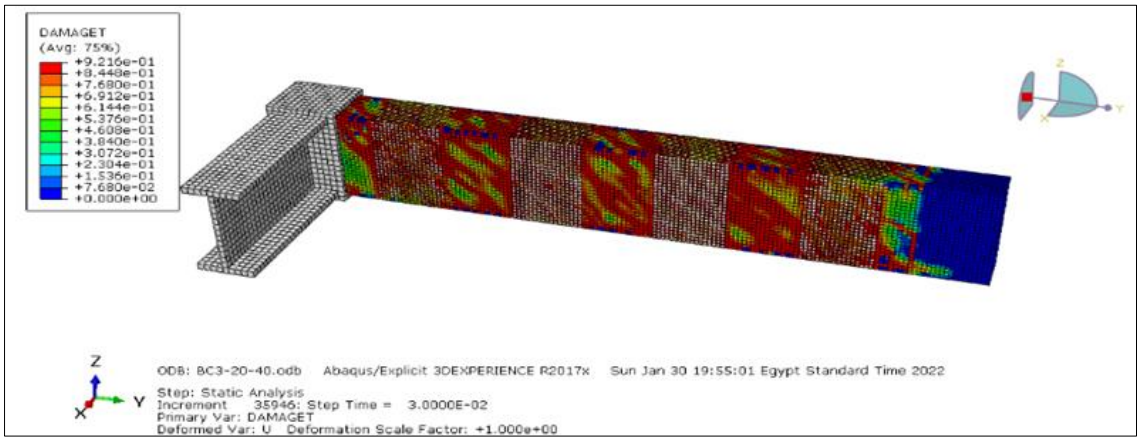

Figure 23 Failure Pattern of FE Model for Strengthened Beam BC3-200-400

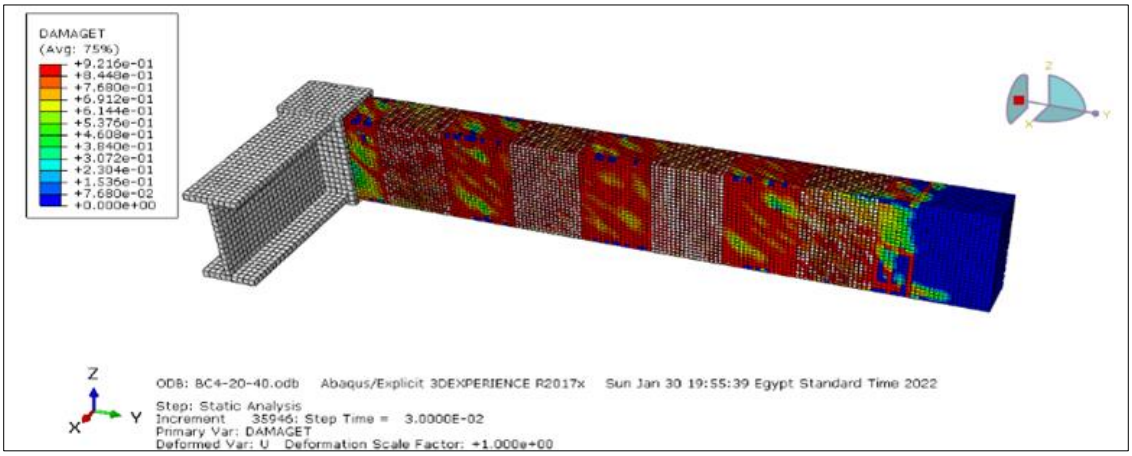

Figure 24 Failure Pattern of FE Model for Strengthened Beam BC4-200-400

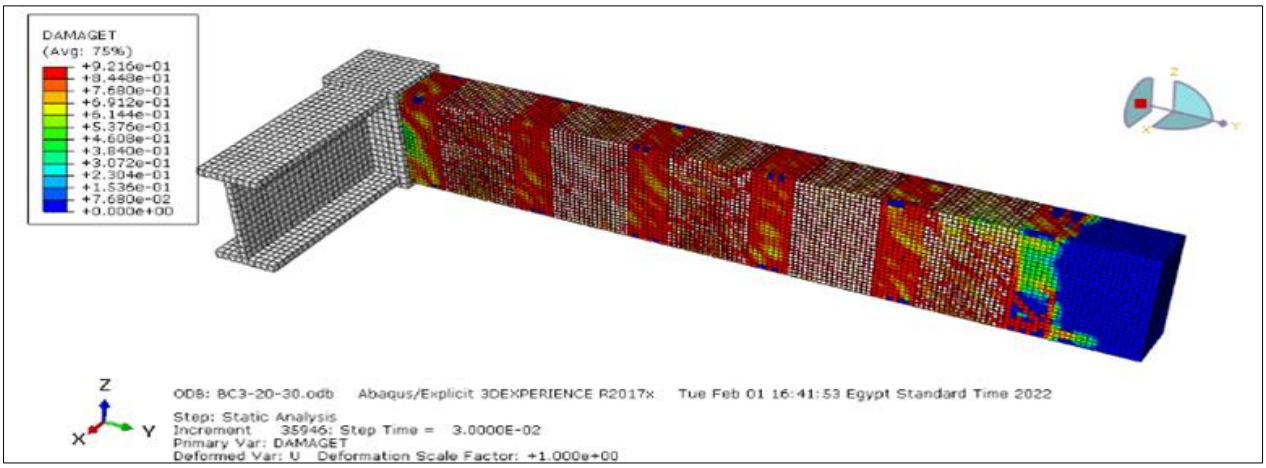

Figure 25 Failure Pattern of FE Model for Strengthened Beam BC3-50-100

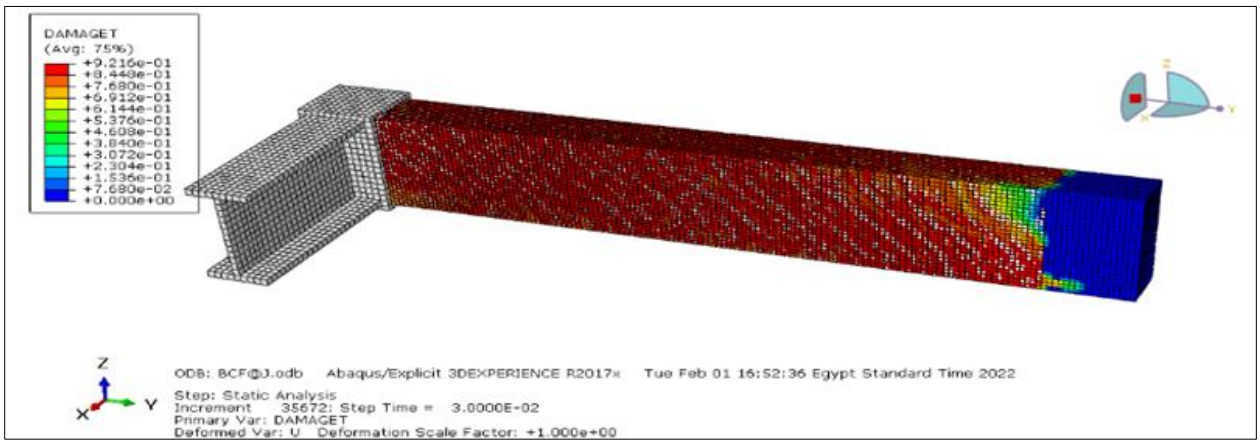

Figure 26 Failure Pattern of FE Model for Strengthened Beam BC2-1600-0

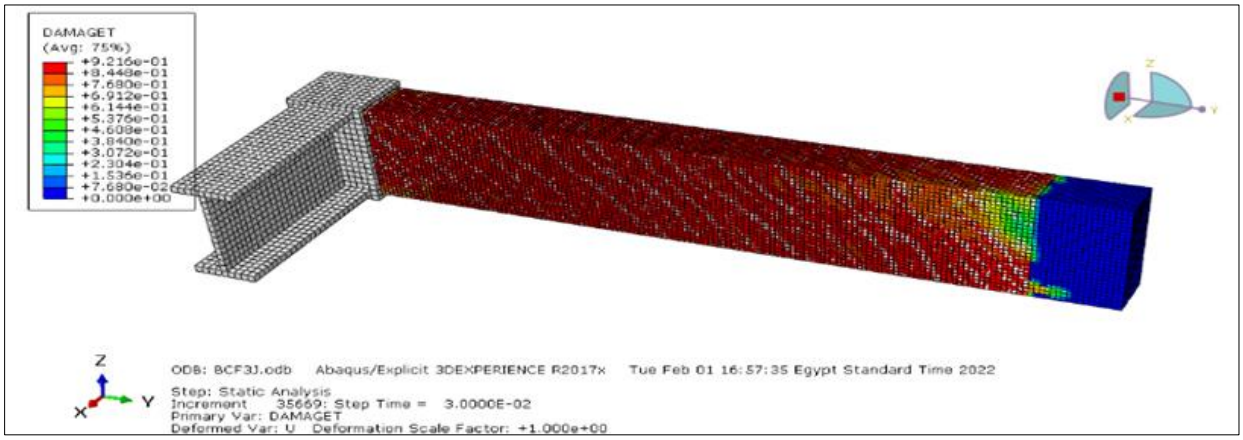

Figure 27 Failure Pattern of FE Model for Strengthened Beam BC3-1600-0

4.3. FRP stress distribution

The stress distribution of CFRP strips and full-wrap models is shown in Figures (28 & 29), revealing that the strips closer to the steel arm generated the maximum stress value.

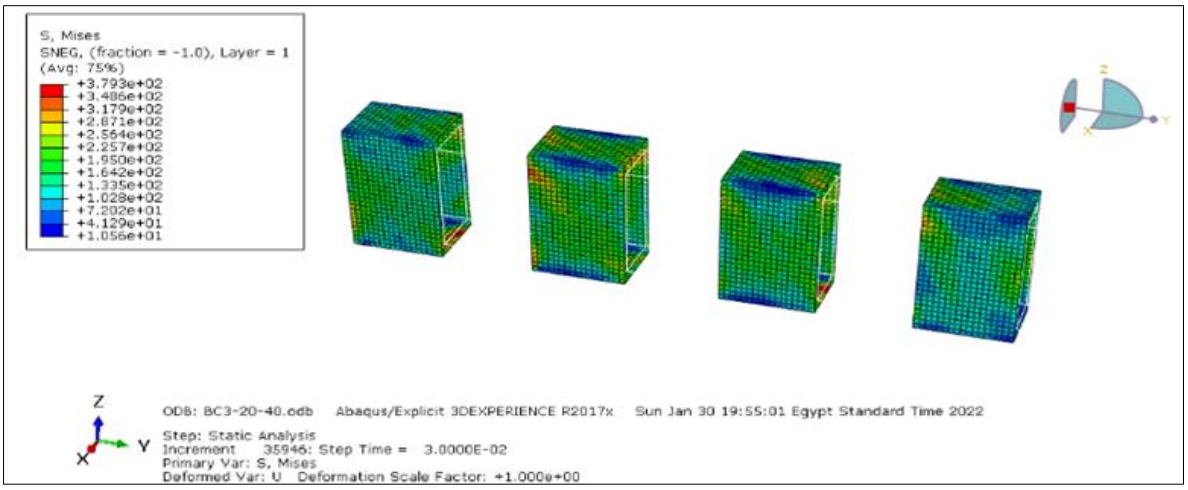

Figure 28 CFRP Strips Stress Distribution

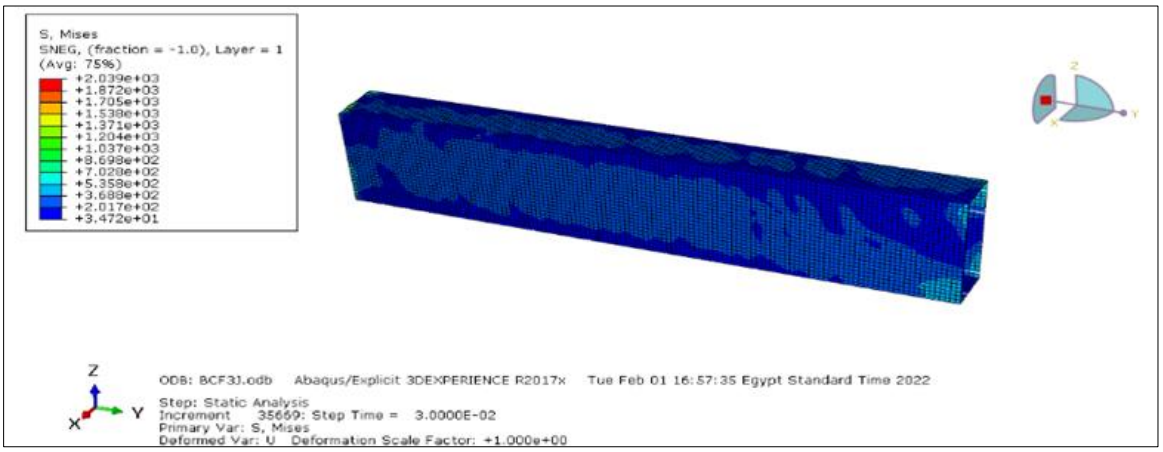

Figure 29 CFRP Full Wrap Stress Distribution

5. Conclusion

- In the present work, the torsion behavior of self-compact reinforced concrete beams has been numerically tested to investigate the impact of self-compact concrete, variable number of layers, and spacing between strips on the torsion behavior of SCC RC beams. The numerical results indicate the following conclusions:
- A FE program (ABAQUS) is suited to simulate the behavior of self-compact RC beams in the nonlinear analysis of 3D RC members under increasing monotonic loads.
- A nonlinear FE method based on ABAQUS-generated 3D models is both economical and powerful as a tool to efficiently simulate the actual behavior of self-compact RC beams subjected to torsional loads.
- The most significant feature of FEM for concrete structures is the selection of adequate and appropriate material models to be used in the numerical simulation. The nonlinear material models on ABAQUS material library provide better results that were generally more realistic, particularly in the case of the Smeared Cracking model employed to model the reinforced concrete.
- The present study attests to the ability of FEA by ABAQUS to predict beams' torsion capacity.

References

[1] N. Y. ELWakkad, Kh. M. Heiza, W. Mansour, Experimental study and finite element modelling of the torsional behavior of self-compacting reinforced concrete (SCRC) beams strengthened by GFRP Case Studies in Construction Materials, 18, 2023. https://doi.org/10.1016/j.cscm.2023. e02123.

[2] JF. Bonacci, M. Maalej, Behavioral trends of RC beams strengthened with externally bonded FRP J. Compos. Constr., 5(2), 102–113, 2001.

[3] C. Pellegrino, C. Modena, Fiber reinforced polymer shear strengthening of reinforced concrete beams with transverse steel reinforcement J. Compos. Constr., 6(2), 2002.

[4] G. B. Maranan, A. C. Manalo, B. Benmokrane, W. Karunasena, P. Mendis, Behavior of concentrically loaded geopolymer-concrete circular columns reinforced longitudinally and transversely with GFRP bars Engineering Structures, 117, 422–436, 2016.

[5] A. De Luca, F. Matta, A. Nanni, Behavior of full-scale glass fiber-reinforced polymer reinforced concrete columns under axial load, ACI Structural Journal, 107(5), 589–596, 2010.

[6] H. Tobbi, A. S. Farghaly, B. Benmokrane, Behavior of concentrically loaded fiber-reinforced polymer reinforced concrete columns with varying reinforcement types and ratios ACI Structural Journal, 111(2), 2014.

[7] H. M. Mohamed, M. Z. Afifi, B. Benmokrane, Performance evaluation of concrete columns reinforced longitudinally with FRP bars and confined with FRP hoops and spirals under axial load Journal of Bridge Engineering, 19(7), 2014.

[8] Heiza, KH. M., Meleka, N.N., and Noha Y. Elwakkad, Behavior and Analysis of Self-Consolidated Reinforced Concrete Deep Beams Strengthened in Shear. ISRN Civil Engineering, Vol. 2012. https://www.researchgate.net/publication/333248718_Behavior_and_Analysis_of_Self-Consolidated_Reinforced_Concrete_Deep_Beams_Strengthened_in_Shear.

[9] Meleka, N.N., Heiza, KH. M., and Noha Y. Elwakkad, Shear Strengthening of Self-Consolidating Reinforced Concrete Deep Beam with a Central Opening. Ain Shams Journal of Civil EngineeringVol. 1.No. 1 ISSN: 1687-8590, 2009.

[10] Meleka, N.N., K. M. Heiza, KH. M., Noha Y. Elwakkad, and Othman, I.M., State-of-the Art Review: Torsional Behavior of RC Beams strengthened by FRP systems Menoufia University, Faculty of Engineering, First International Conference (Ninth Conference of Sustainable Environmental Development), 24-28 March 2017.

[11] Noha Y. Elwakkad, and KH. M. Heiza, Failure Analysis of Strengthened Continuous Reinforced Concrete Beams under Repeated Load, 2nd International Conference in Innovative Building Materials, Housing and Building national Research Center (HBRC), 2 -4 December 2018, Cairo, Egypt.

[12] Noha Y. Elwakkad, KH. M. Heiza, M. Elmahroky, and Aqeel Al-Adili, literature Review for Strengthening of Existing Reinforced Concrete Structures using Steel and FRP Plates, Menoufia University, Faculty of Engineering, Second International Conference, (Tenth Conference of Sustainable Environmental Development) 16-20 March 2019, Sharm El Sheikh, Egypt.

[13] Noha Y. Elwakkad, KH. M. Heiza, and M. Elmahroky, State of the Art Review on Strengthening of Reinforced Concrete Structures using Near Surface Mounted Technique, Menoufia University, Faculty of Engineering, Second International Conference, (Tenth Conference of Sustainable Environmental Development) 16-20 March 2019, Sharm El Sheikh, Egypt.

[14] Noha Y. Elwakkad, and KH. M. Heiza, Failure Analysis of Strengthened Continuous Reinforced Concrete Beams under Repeated Load, Menoufia University, Faculty of Engineering, Second International Conference, (Tenth Conference of Sustainable Environmental Development) 16-20 March 2019, Sharm El Sheikh, Egypt.

[15] Noha Y. Elwakkad, Behavior of reinforced self-curing concrete slabs exposed to fire, Journal of Engineering Sciences (JES), Faculty of engineering- Assuit university, part A-ciivil engineer, July 2023. https://dx.doi.org/10.21608/jesaun.2023.212300.1231.

[16] M. Ameli, H. R. Ronagh, P. F. Dux, Behavior of Strengthened Reinforced Concrete Beams under Torsion Journal of Composites for Construction, 11(4), 192–200, 2007.

[17] P. Salom, J. Gergely, D. Young, Torsional retrofit of spandrel beams with composite laminates Journal of Composites for Construction (ASCE), 8(2), 157–162, 2004.

[18] A. Ghobarah, M. N. Ghorbel, S. E. Chidiak, Upgrading torsional resistance of reinforced concrete beams using fiber reinforced polymer Journal of Composites for Construction (ASCE), 6(4), 257–263, 2002.

[19] A. Ghobarah, FRP composites in civil engineering. Proc. FRP composites in civil engineering CICE, Hong Kong, vol. 1. p. 701–712, 2001.

[20] S. Panchacharam, A. Belarbi, Torsional behavior of reinforced concrete beams strengthened with FRP composites First FIB Congress, Osaka, Japan, 1, October 13-19, 2002.

[21] M. A. El-Mandouh, M. S. Omar, A. S. Abd El-Maula, Behaviour of RC flat slabs with openings strengthened with CFRP Case Stud. Constr. Mater., 15, 2021.

[22] M. Mazloom, M. Mehrvand, P. Pourhaji, A. Savaripour, Studying the effects of CFRP and GFRP sheets on the strengthening of self-compacting RC girders, Struct. Monit. Maint., 6(1), 47-66, 2019.

[23] L. F. Silva, E. S. Filho, J. J. Filho, Torsional behavior of RC beams strengthened with carbon fiber reinforced polymer composites Adv. Struct. Eng., 24(9), 2027–2041, 2021.

[24] Abaqus Documentation User's Guide, ABAQUS User's Guide: Dassault Syst`emes, Simulia Corp Providence, 2014.

[25] Ngo D, Scordelis AC., Finite element analysis of reinforced concrete beams, ACI J 1967, 64(3).

[26] H. K. Lee, B. R. Kim, S. K. Ha, Numerical evaluation of shear strengthening performance of CFRP sheets/strips and sprayed epoxy coating repair systems Compos B Eng., 39(5), 851–62, 2008.

[27] S. S. Prakash, A. Belarbi, Y. M. You, Seismic performance of circular RC columns subjected to axial, bending, and torsion with low and moderate shear Eng. Struct. Elsevier, 32(1), 46–59, 2010.

[28] R. Santhakumar, R. Dhanaraj, E. Chandrasekaran, Behaviour of retrofitted reinforced concrete beams under combined bending and torsion: a numerical study Electronic Journal of Structural Engineering, 7, 1–7, 2007.

[29] E. Higazy, M. El-Kateb, Experimental and Numerical Investigation on Torsional Strengthening of Reinforced Concrete Beams Using FRP Sheets September, 2012. https://www.researchgate.net/publication/233926982_Experimental_and_Numerical_Investigation_on_Torsional_Strengthening_of_Reinforced_Concrete_Beams_Using_FRP_Sheets.

[30] I. M. H. Alshaikh, B. H. Abu Bakar, E. A. H. Alwesabi, A. M. Zeyad, H. M. Magbool, Finite element analysis and experimental validation of progressive collapse of reinforced rubberized concrete frame Structures, 33, 2361–2373, 2021.

[31] A. Altheeb, I. M. H. Alshaikh, A. A. Nehdi, H. Alghamdi, Effects of non-structural walls on mitigating the risk of progressive collapse of RC structures Lat. Am. J. Solids Struct., 19(3), 1-18, 2022.

[32] I. AL-Shaikh, N. Falah, Numerical analysis of masonry-infilled reinforced concrete frames J. Sci. Technol., 19(2), 2014.

[33] G. Zhao, A. Li, Numerical study of a bonded steel and concrete composite beam Comput. Struct. J., 86(19–20), 1830–1838, 2008.

[34] https://egy.sika.com/content/dam/dms/eg01/h/sikawrap_-230_c.pdf